Surface Science 602 (2008) 2758–2768

Contents lists available at ScienceDirect

Surface Science

journal homepage: www.elsevier.com/locate/susc

First-principles studies of H_2S adsorption and dissociation on metal surfaces

Dominic R. Alfonso *

National Energy Technology Laboratory, US Department of Energy, P.O. Box 10940, Pittsburgh, PA 15236, United States
Parsons Project Services, Inc., South Park, PA 15129, United States

ARTICLE INFO

Article history:
Received 23 April 2008
Accepted for publication 1 July 2008
Available online 10 July 2008

Keywords:
Chemisorption
Density functional theory calculations
Sulfur
Metallic surfaces
Adatoms
Low index single crystal surfaces

ABSTRACT

Density functional theory calculations were employed to investigate the molecular and dissociative adsorption of H_2S on the closed packed surfaces of a number of important noble metals (Ag(111), Au(111) and Cu(111)) and transition metals (Ir(111), Ni(111), Pd(111) and Pt(111)). Energy minima corresponding to adsorbed states were identified with H_2S binding preferentially at the top sites. The adsorption of other S moieties (SH and S) was also examined. SH and S were found to prefer bridge sites and hollow sites, respectively. The binding of H_2S and its S-containing dissociated species is stronger on the transition metals. The elementary reactions of abstraction of H from H_2S to form a surface SH intermediate and abstraction of H from SH to form a surface S intermediate as model pathways for the dissociation of H_2S were examined. Our results suggest that H_2S decomposition on the aforementioned transition metal surfaces is more facile, both thermodynamically and kinetically.

1. Introduction

The interaction of H_2S with metal surfaces is of considerable interest due primarily to two reasons. Technologically, it is a relevant reaction in areas such as hydrodesulfurization of hydrocarbons [1] and gas sensors [2,3]. Scientifically, it is widely used as a model system to understand the various reasons for the poisoning of metals by sulfur compounds. Major S contaminants, such as H_2S (which is a common impurity in fossil derived fuels and chemical feedstocks), have highly poisonous effects on metal-based catalysts encountered in many chemical reactions in the petrochemical industry. Metal-based membranes that are used for separation of hydrogen produced from hydrocarbon reforming and water–gas shift reactions also suffer from a similar problem [4,5]. It was found that H_2S in the process streams deactivates the metal membranes giving rise to reduction in their selectivity and hydrogen permeability. Uncontrollable and accidental poisoning of these materials could incur great cost to the economy [6]. It is hoped that fundamental understanding of the H_2S–metal chemistry would help characterize the problem and likewise would provide insights for the development of S-resistant catalysts and membrane materials.

Experimental studies of interaction of H_2S with close-packed transition and noble metal surfaces (Ag(111) [7], Au(111) [8], Co(0001) [9], Cu(111) [10] and Pt(111) [11]) as well as with the corresponding open surfaces (Ag(100) [12,13], Au(100), Au(110) [14–16], Cu(100) [17], Mo(100) [18], Ni(100) [19–21], Ni(110) [22], Pd(100) [23], Rh(100) [24], Ru(110) [25], W(100) [26]) were reported. A variety of techniques such as low-energy electron diffraction (LEED), scanning tunneling microscopy (STM), X-ray photoemission spectroscopy (XPS), normal incidence X-ray standing wave (NIXSW) analysis, temperature program desorption (TPD), high-resolution electron energy loss spectroscopy (HREELS) and Auger electron spectroscopy (AES) were utilized. From this body of work has emerged a picture of facile H_2S dissociation on most of these metals at low temperatures (generally below ~185 K). The major exceptions are Ag(111), Ag(100), Au(111), Au(100) and Cu(111) surfaces which, in comparison, were found to be inefficient in dissociating H_2S particularly at low temperatures [7,10,12–16].

Adsorption of H_2S at room temperature and above giving rise to sulfidation of the metals has also been experimentally studied in some detail. These efforts have included work on close-packed surfaces of transition (Co(0001) [9], Ru(0001) [27–30], Ir(111) [31], Ni(111) [32–35], Pd(111) [36–40], Pt(111) [41–44], Rh(111) [45–47]) and noble metals (Ag(111) [12,48,49], Au(111) [50–52], Cu(111) [53–55]). The formation of $(\sqrt{3} \times \sqrt{3})$ $R30°$ structure on the (111) surfaces was frequently observed while the (2×2) structure was commonly reported on the (0001) face. These structures were determined to consist of S overlayer with one S atom per unit mesh on an essentially undistorted metal substrate. Formation of far more "complex" S phases was found with increase H_2S dosing or post-annealing to above room temperatures. This generally involves a far more disruption of the metal substrate with some kind of reconstruction of the outermost layer giving rise

* Address: National Energy Technology Laboratory, US Department of Energy, P.O. Box 10940, Pittsburgh, PA 15236, United States. Tel.: +1 412 386 4113; fax: +1 412 386 4542.
E-mail address: alfonso@netl.doe.gov

0039-6028/$ - see front matter © 2008 Elsevier B.V. All rights reserved.
doi:10.1016/j.susc.2008.07.001

to mixed metal–sulfur overlayer structure. Despite the enormous experimental efforts, knowledge of the chemistry of H_2S on these metals is rather limited despite the fact that it is known that the decomposition of the gas molecules is a fundamental step in the sulfidation process. Some basic questions such as the adsorption geometries and dissociation pathways of H_2S are not completely clarified experimentally. The difficulty in experiments may be attributed to the generally fast kinetics of H_2S dissociation on metals. Consequently, this impedes detailed structural and mechanistic elucidation of the adsorption and the dissociation process.

From the theoretical standpoint, first-principles investigations focusing on the behavior of H_2S on metals using periodic supercells are also somewhat scarce but some strides have nonetheless begun to be made. This type of study is a valuable complement to experimental efforts since it allows direct observation of some atomic-scale phenomena which cannot be achieved in current experimental techniques. For example, with periodic density functional theory (DFT) techniques, preliminary investigations of the adsorption and dissociation of H_2S on Pd(1 1 1) were carried out [56]. Adsorption energy and geometry of H_2S plus its dissociation products, S and SH, were reported. The dissociation pathways, including thermochemistry and reaction barrier were also addressed. The dissociation of H_2S was found to have low barriers and high exothermicities. Similar studies on the corresponding Ni(1 1 1), Fe(1 0 0) and Fe(1 1 0) surfaces were also performed [57–59]. The decomposition of H_2S on these surfaces was also predicted to be a facile process.

The present work was undertaken to further improve our understanding of the behavior of H_2S on metal surfaces. We report here a systematic investigation of H_2S adsorption and decomposition on several important close-packed transition and noble metal surfaces (Ag(1 1 1), Au(1 1 1), Cu(1 1 1), Ir(1 1 1), Ni(1 1 1), Pd(1 1 1) and Pt(1 1 1)) using a consistent theoretical scheme. In particular, we examined the binding properties of H_2S and its dissociation products. Additionally, mechanistic aspect of the dissociation of this molecule on the different metal surfaces was characterized, with particular attention given to the thermochemistry and reaction barriers. The rest of the manuscript is organized as follows. The technical details of the calculations were outlined in Section 2. We presented the adsorption structure and binding energy of H_2S and the various intermediates, SH, S and H, in Section 3.1. The predicted pathways for H_2S dissociation were given in Section 3.2. Our conclusions were drawn in the final section.

2. Computational approach

First-principles DFT total energy calculations were carried out as implemented in the Vienna Ab initio Simulation Package (VASP) code [60,61]. This implementation includes total energy and atomic force calculations. We used the generalized gradient approximation (GGA) formulation of Perdew, Burke and Enzerhoff (PBE) [62] to calculate the exchange-correlation energy. The electron–ion interaction was described by the projector-augmented wave (PAW) method [63]. The Kohn–Sham one electron valence eigenstates were expanded in terms of plane-wave basis sets with a cutoff energy of 280 eV.

The Ag(1 1 1), Au(1 1 1), Cu(1 1 1), Ir(1 1 1), Ni(1 1 1), Pd(1 1 1) and Pt(1 1 1) surfaces were represented by a five-layer slab with periodic boundary conditions in the two directions parallel to the surface. In order to ensure the decoupling of the consecutive slabs, a 15 Å thick vacuum region is employed. A (3×3) surface unit cell was used where there are nine metal atoms in each layer. For each surface, the lattice constant was fixed to the value obtained from optimizing with DFT this constant for the bulk metal. The computed lattice constants for the bulk Ag, Au, Cu, Ir, Ni, Pd and Pt are 4.17, 4.18, 3.64, 3.88, 3.52, 3.97 and 3.98 Å, respectively. The corresponding experimental values are 4.09, 4.08, 3.61, 3.84, 3.52, 3.89 and 3.92 Å, respectively [64]. Our predictions are found to within ~2% of the measured values.

Adsorption of H_2S and its dissociation products, SH, S and H, is allowed on one side of the slab. The electrostatic potential is adjusted accordingly [65]. A set of geometry optimizations were performed by placing the adsorbate at one of the high symmetry adsorption site on the surface (top, bridge, fcc and hcp sites). For H_2S and SH, different initial orientations and distances with respect to the surface were explored. During the geometry optimization, the coordinates of the top three metal layers and the adsorbate were allowed to relax while the bottom two layers were fixed to their calculated bulk positions. The k-point sampling of the two-dimensional electronic Brillouin zone of the periodic supercells was performed using the Monkhorst–Pack scheme [66]. We used Monkhorst–Pack mesh of $3 \times 3 \times 1$. A Methfessel–Paxton smearing [67] of $\sigma = 0.2$ eV was utilized to improve convergence and the corrected energy for $\sigma \to 0$ was employed. Spin polarization effects are tested and included where appropriate. Previously, we carried out preliminary investigations of the behavior of H_2S on Pd(1 1 1) [56]. In that work, we used the Perdew–Wang (PW91) GGA functional to compute the exchange-correlation energy [68]. Core orbitals were described by non-local reciprocal space space ultra-soft pseudopotentials in the Vanderbilt form [69]. For the sake of consistency, we reexamined this system using exactly the same calculational setup employed here.

The adsorption energy of the adsorbate species, E_{ads}, was calculated using the expression

$$E_{ads} = E_{adsorbate+slab} - (E_{slab} + E_{adsorbate}) \quad (1)$$

where $E_{adsorbate+slab}$ is the total energy of the relaxed adsorbate-surface system, while E_{slab} and $E_{adsorbate}$ are the total energy of the relaxed bare surface and gas phase adsorbate respectively. $E_{adsorbate}$ was calculated by placing a molecule or an atom in a cubic box with dimensions of 15 Å sides and performing spin-polarized Γ-point calculations. Based on this definition, a negative E_{ads} indicates that the adsorption is exothermic. Adsorption energies and site preferences for the H_2S, SH, S and H were described for 1/9 ML coverage. Our analysis would focus primarily on the most favorable adsorption mode for each type of adsorbate but data on the other stable configurations would be provided as well.

The dissociation pathway studied here involves sequential abstraction of H atoms from H_2S [56–59]. This sequential S–H scission gives rise to surface SH and surface S intermediates (i.e. $H_2S_{(ad)} \to SH_{(ad)} + H_{(ad)}$ and $SH_{(ad)} \to S_{(ad)} + H_{(ad)}$). We investigated the thermochemistry and identified the transition state for each elementary step. The minimum energy pathway for each reaction step was mapped out using the nudged elastic band (NEB) technique [70,71]. NEB is a method for finding saddle points and minimum energy paths between known reactants and products. A discrete representation of the reaction path was employed, with the points (movable images) along the path being relaxed using first derivative information only. In this work, five images were used in the search for the saddle point of each elementary reaction step mentioned above. An initial chain of images is constructed between the initial reactants and final reaction products using linear interpolation between the two endpoints. The energies of the images and the endpoints were obtained from spin-polarized calculations. The transition state of the optimized reaction coordinate was approximated by the image of highest energy. The overall reaction energy ΔE_{rxn} was calculated using the expression

$$\Delta E_{rxn} = \sum E_{prod} - \sum E_{react} \quad (2)$$

where the first and second terms represent the sum of energies of products and reactants, respectively. Based on this convention, a negative ΔE_{rxn} corresponds to an exothermic reaction.

3. Results and discussion

3.1. Adsorption of H_2S, SH, S and H on the metal surfaces

The computed adsorption energies and optimized structural parameters for H_2S adsorption on the different metal surfaces are tabulated in Table 1. In all cases, energy minima corresponding to adsorbed states were identified. Binding on the top site is favored with adsorption energy that varies from −0.17 to −0.91 eV with respect to the gas phase molecule. In this configuration, the molecule binds to the metal surfaces through its sulfur atom (Fig. 1a). The calculated S–metal distance varies from 2.21 to 2.82 Å, The adsorbed molecule lies nearly parallel to the surface, the angle between the surface plane and the S–H bond axis being 4–14°. The internal structure of the adsorbed H_2S is only slightly deformed with respect to its gas phase counterpart. The H–S–H internal angles and S–H bondlengths are 91–92° and 1.36–1.37 Å, respectively. The corresponding gaseous values are 93° and 1.35 Å, respectively. It can be seen from Table 1 that the adsorption energy is larger for the transition metal surfaces, namely, Ir(1 1 1), Ni(1 1 1), Pd(1 1 1) and Pt(1 1 1) (E_{ads} = −0.56 to −0.91 eV), compared to the noble metal surfaces (E_{ads} = −0.17 to −0.27 eV). For all the studied metals, the rotation of H_2S about the S–metal bond has a very small effect on the total energy. The energy was found to change by less than 0.01 eV suggesting that that the molecule is free to rotate on the surface. We also looked at the energetics for the case where the metal surfaces are rigid and the molecule is non-deformable. That is, the adsorption energy was calculated with the metal substrate and H_2S fixed to their calculated bulk/gas phase positions. The corresponding E_{ads} was predicted to be reduced by 17–62%. The calculated values are −0.14, −0.20, −0.10, −0.34, −0.35, −0.57 and −0.67 eV on Ag(1 1 1), Au(1 1 1), Cu(1 1 1), Ir(1 1 1), Ni(1 1 1), Pd(1 1 1) and Pt(1 1 1), respectively. This indicates that the contribution of the substrate and the adsorbate relaxation to the values reported in Table 1 is quite significant.

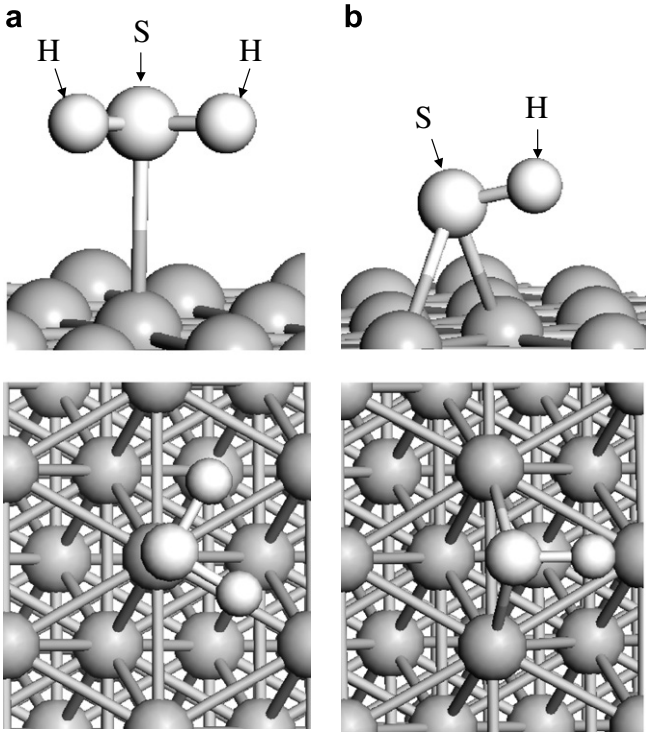

Fig. 1. Basic structure of: (a) H_2S adsorbed on the top site, and (b) SH adsorbed on the bridge site of the metal surfaces.

With the exception of Ag(1 1 1) and Au(1 1 1), bridge site was found to be stable adsorption site. However, it is disfavored by 0.06–0.40 eV relative to the top site adsorption. In this configuration, the molecular plane of the adsorbate is perpendicular to the

Table 1
Adsorption properties of H_2S on the close packed surfaces of various metals

	Site	E_{ads} (eV)	$d_{S-metal}$ (Å)	d_{S-H} (Å)	$\angle_{Surf-S-H}$ (°)	$\angle_{H-S-H}$ (°)
Ag(1 1 1)						
	Top	−0.17(−0.3)[a]	2.82	1.36	6	92
	Bridge	–	–	–	–	–
Au(1 1 1)						
	t+op	−0.27(−0.4 to −0.5)[b]	2.62	1.36	4	92
	Bridge	–	–	–	–	–
Cu(1 1 1)						
	Top	−0.26(−0.3–0.4)[c]	2.40	1.36	10	92
	Bridge	−0.05	2.40	1.37	43	95
Ir(1 1 1)						
	Top	−0.77	2.34	1.37	13	91
	Bridge	−0.49	2.31	1.38	42	95
Ni(1 1 1)						
	Top	−0.56	2.21	1.37	14	91
	Bridge	−0.50	2.18	1.38	43	94
Pd(1 1 1)						
	Top	−0.75	2.31	1.37	10	92
	Bridge	−0.61	2.33	1.37	43	93
Pt(1 1 1)						
	Top	−0.91	2.30	1.37	11	91
	Bridge	−0.51	2.30	1.37	42	96
	$H_2S_{(g)}$[d]			1.348(1.328)[e]		92.8,(92.2)[e]

Listed are the: adsorption energy per H_2S molecule (E_{ads}), S–metal bondlength ($d_{S-metal}$), S–H bondlength (d_{S-H}), H–S–H bond angle ($\angle_{H-S-H}$) and the angle between the surface plane and the S–H bond ($\angle_{Surf-S-H}$). Where comparison is available, experimental values are given in parenthesis.

[a] Ref. [7].
[b] Ref. [8].
[c] Ref. [10].
[d] For reference purposes, the computed and experimental structural properties of the gas phase H_2S are also provided.
[e] Ref. [96].

surface. It binds to the surfaces through its sulfur atom with the H atoms directed towards the gas phase. In the case of the fcc and hcp sites, they are predicted to be unstable for all the examined metals. We found that the adsorbed molecule eventually relaxed towards the bridge sites after being initially placed at the hollow sites. The preference for top site adsorption predicted here for H_2S can be explained by analogy to gas phase bonding as suggested in previous work [72]. H_2S is stable in the gas phase. Hence, the lowest possible coordination is expected in the adsorbed state.

The behavior of H_2S on the clean Ag(1 1 1) surface was studied previously by means of TPD [7]. At 80 K, molecular adsorption was observed. On Au(1 1 1), Cu(1 1 1) and Pt(1 1 1), molecular adsorption was reported at 85 K, 120 K and 110 K, respectively, on the basis of TPD and XPS [8,10,11]. Our study offers theoretical confirmation that molecular H_2S adsorption on Ag(1 1 1), Au(1 1 1), Cu(1 1 1) and Pt(1 1 1) is stable. There is no direct information about the geometry of the adsorbed H_2S from these experiments to compare with our finding. On Ir(1 1 1) [31], Ni(1 1 1) [32–35] and Pd(1 1 1) [36–40], previous experimental efforts primarily focused on the sulfidation of the surfaces via room temperature exposure to H_2S. At this condition, no evidence of molecular adsorption was observed because H_2S was found to dissociate quickly giving rise to adsorbed S species. To our knowledge, low temperature characterization of H_2S adsorption on Ir(1 1 1), Ni(1 1 1) and Pd(1 1 1) has never been attempted experimentally. Our work provides a theoretical confirmation that the adsorption of H_2S on these surfaces is energetically favorable.

Investigations of H_2S adsorption on Cu(1 1 1) [73], Ni(1 1 1) [73,74] and Pt(1 1 1) [75] were previously carried out using DFT based on a (2×2) slab (θ_{H_2S}=1/4 ML). These studies also concluded that H_2S binds through the S atom at a top site with the molecule sitting almost flat on the surface. DFT studies of H_2S adsorption on Ni(1 1 1) and Pd(1 1 1) at θ_{H_2S} = 1/9 ML employing a 3–4 layer (3×3) slab were reported [56,57]. These works lead to similar conclusions: i.e. the top site is the most favorable and the molecule is nearly parallel to the surface. Our values for H_2S adsorption on Ni(1 1 1) and Pd(1 1 1) can be compared with the above calculations The reported top site adsorption energy on Ni(1 1 1) and Pd(1 1 1) are −0.55 and −0.73 eV, respectively. These compare well with our calculated values of −0.56 eV and −0.75 eV, respectively.

Redhead analysis of the TPD spectra of H_2S desorption from Ag(1 1 1) yields an estimated adsorption energy of ∼−0.3 eV [7]. TPD was also used to determine the adsorption energy of H_2S on Au(1 1 1) and Cu(1 1 1) and Redhead analysis of the data gives a value of ∼−0.4 to ∼−0.5 eV [8] and ∼−0.3 to ∼−0.4 eV [10], respectively. These values are somewhat larger than our computed H_2S adsorption energy on Ag(1 1 1), Au(1 1 1) and Cu(1 1 1) of −0.17, −0.27 and −0.26 eV, respectively. However, it must be emphasized that the results of comparison of the predicted adsorption energies from those obtained by TPD experiments must be interpreted with some caution. As pointed out in Refs. [76,77], interpretation of TPD data requires the knowledge of frequency prefactor which is often unknown. Thus, determination of adsorption energies from TPD experiments is often based on some guessed value for the prefactor which is typically 10^{13} s^{-1}. This guessed prefactor, on the other hand, could be orders of magnitude from the correct value.

In Table 2, we list the adsorption energies and structural properties for SH on the stable sites of the various metal surfaces. Similar to H_2S, SH was found to bind to the substrate through the S atom. However, in contrast to H_2S, SH interacts more strongly with the studied metals. It is seen that SH prefers the bridge site (Fig. 1b). Adsorption on the hollow sites is predicted to be stable but the adsorption energies were found to be ∼0.2 to ∼0.7 eV weaker. For hollow site adsorption, SH binds with the axis of the species perpendicular to the surface plane. On Au(1 1 1), Ir(1 1 1) and Pt(1 1 1), SH exhibits stable top site adsorption but they are also found to be less stable compared to the bridge site (adsorption is ∼0.4 to ∼0.7 eV stronger in the bridge site). In this configuration, the SH bond axis is inclined with respect to the surface plane with the S atom bound to the surface. Unlike H_2S, the most preferred binding site predicted for SH suggests that gas phase bonding trends are not followed by this species on the different surfaces considered here. SH binds to at most one atom in the gas phase. Hence, it is expected to be onefold coordinated to the surface in the adsorbed state, yet it is preferentially adsorbed on the twofold bridge site.

Table 2
Adsorption properties of SH on the close packed surfaces of various metals

Site	E_{ads} (eV)	$d_{S-metal}$ (Å)	d_{S-H} (Å)	$\angle_{Surf-S-H}$ (°)
Ag(1 1 1)				
Top	–	–	–	–
Bridge-fcc	−2.34	2.56	1.37	10
Bridge-hcp	−2.34	2.54	1.36	12
fcc	−2.16	2.54	1.37	90
hcp	−2.11	2.55	1.37	90
Au(1 1 1)				
Top	−1.88	2.37	1.36	8
Bridge-fcc	2.23	2.47	1.37	9
Bridge-hcp	−2.23	2.47	1.37	11
fcc	−1.94	2.46	1.38	90
hcp	−1.77	2.49	1.37	90
Cu(1 1 1)				
Top	–	–	–	–
Bridge-fcc	−2.76	2.29	1.37	14
Bridge-hcp	−2.76	2.29	1.37	13
fcc	−2.53	2.26	1.37	90
hcp	−2.50	2.27	1.37	90
Ir(1 1 1)				
Top	−2.49	2.29	1.37	12
Bridge-fcc	−3.22	2.34	1.40	11
Bridge-hcp	−3.20	2.35	1.39	13
fcc	−2.89	2.30	1.39	90
hcp	−2.76	2.30	1.39	90
Ni(1 1 1)				
Top	–	–	–	–
Bridge-fcc	−3.27	2.17	1.52	2
Bridge-hcp	−3.22	2.17	1.50	3
fcc	−2.90	2.15	1.38	90
hcp	−2.84	2.15	1.38	90
Pd(1 1 1)				
Top	–	–	–	–
Bridge-fcc	−3.37	2.29	1.44	6
Bridge-hcp	−3.29	2.30	1.39	14
fcc	−3.05	2.27	1.38	90
hcp	−2.94	2.29	1.38	90
Pt(1 1 1)				
Top	−2.48	2.26	1.37	10
Bridge-fcc	−3.18	2.31	1.40	8
Bridge-hcp	−3.15	2.31	1.39	13
fcc	−2.86	2.27	1.38	90
hcp	−2.51	2.29	1.39	90
$SH_{(g)}$[a]			1.35(1.345)[b]	

Listed are the: adsorption energy per SH (E_{ads}), S–metal bondlength ($d_{S-metal}$), S–H bondlength (d_{S-H}) and the angle between the surface plane and the S–H bond ($\angle_{Surf-S-H}$).
[a] For reference purposes, the computed and experimental structural properties of a gas phase SH are also provided.
[b] (Ref. [96]).

For clarity, two types of bridge site termed bridge-fcc and bridge-hcp were reported. The bridge-fcc (bridge-hcp) site corresponds to a binding situation in which the S–H bond lies above the fcc (hcp) site. On Ag(1 1 1), Au(1 1 1), Cu(1 1 1), Ir(1 1 1) and Pt(1 1 1), the adsorbate at both bridge-fcc and bridge-hcp sites binds in a typical twofold bridge configuration. The S–H bond retains a length close to the gas phase value (within 0.05 Å). The difference in the energy for the two types of bridge site is ⩽0.03 eV. On Pd(1 1 1), SH on bridge-hcp site also essentially binds in a typical bridge fashion. For bridge-fcc site adsorption, it binds such that

S atom is displaced approximately between the bridge and the fcc site. The H atom exhibits a top-like interaction with a metal atom giving rise to elongation of the S–H bond by 0.09 Å with respect to the gas phase value. The bridge-fcc site is preferred by 0.08 eV compared to bridge-hcp site. This type of binding configuration was also seen for both types of bridge site adsorption on Ni(1 1 1). The S–H bond is stretched by 0.15–0.17 Å with respect to the gas phase value. Binding on the bridge-fcc site is slightly preferred by 0.05 eV with respect to the bridge-hcp site. It can be seen in Table 2 that the bridge site SH adsorption on transition metal surfaces (E_{ads} = −3.22 to −3.37 eV), is stronger than on noble metals (E_{ads} = −2.23 to −2.76 eV).

Except for Pt(1 1 1), we are not aware of any experimental characterization of SH on the surfaces examined here. Adsorbed SH was observed on Pt(1 1 1) by HREELS and this species was found to be stable on the surface up to 150 K [11]. It was inferred that SH may be inclined on Pt(1 1 1) based on the HREELS analysis. Our predicted most stable structure for SH on Pt(1 1 1) is in line with this observation. Theoretical studies of SH interaction with some of the metal surfaces considered here are somewhat more common. Previous DFT studies found the same preferred site and binding configuration for SH on Pt(1 1 1) at θ_{SH} = 1/4 ML [75]. Using DFT, examination of SH adsorption on Ni(1 1 1) at 1/9 ML coverage was reported [57]. The bridge-fcc and bridge-hcp sites were found to be the lowest in energy which is in line with our findings. It was also observed that the S atom sits approximately between the bridge and the fcc (hcp) site with the H atom exhibiting a top-like interaction with a metal atom. Their reported adsorption energies for bridge-fcc and bridge-hcp based on a four layer slab model are −3.17 and −3.09 eV, respectively. Our calculated values of −3.27 and −3.22 eV are somewhat larger than these. Presumably, this could be attributed to the differences between the calculational details underlying these two studies. In our earlier preliminary work, we primarily focused on SH bound Pd(1 1 1) in a typical twofold bridge configuration which we calculated to be at best metastable on the surface [56]. In the present work, we identified a stable bridge-fcc site adsorption where S is situated between the bridge and the fcc site and H shows a top-like interaction with a Pd surface atom.

The computed S adsorption energies and the distance from the adsorbate to the neighboring metal atoms are presented in Table. 3. A consistent preference for threefold hollow sites is observed with the fcc site more favorable over the hcp site by 0.04–0.25 eV. The calculated S–metal distance in threefold sites varies from 2.14 to 2.46 Å. S hollow site adsorption on transition metal surfaces is found to be stronger (E_{ads} = −5.17 to −5.57 eV) in comparison to the noble metals (E_{ads} = −3.94 to −4.75 eV). It should also be noted that the adsorption energies of the S-containing species in their most stable configuration on a given surface increase in the following sequence: H_2S < SH < S.

The calculated preference of S for fcc site in Au(1 1 1), Ir(1 1 1), Ni(1 1 1), Pd(1 1 1) and Pt(1 1 1) is consistent with previous experimental works [31,33,36,37,41,42,52,78–81]. Additionally, the corresponding structural parameters calculated for S adsorption on these metals agree well with the experimental data. For example, on Au(1 1 1), experimental measurements suggest a S–Au metal bondlength of 2.4 Å [52] in agreement with our calculated value of 2.39 Å. On Ir(1 1 1), the S–Ir bondlength estimated from LEED measurements is 2.28 Å [31] which compares well with our calculated value of 2.31 Å. The S–Ni bondlength observed in our calculations is 2.14 Å and the corresponding SEXAFS and LEED values are 2.13–2.23 Å [35,78,79]. On Pd(1 1 1), SEXAFS and LEED were used to measure a S–Pd bondlength of 2.28 [81] and 2.23 Å [36,37], respectively. They compare well with our computed value of 2.24 Å. On Pt(1 1 1), the LEED determined S–Pt distances of 2.24–2.28 Å [41,42] agree well with our calculated values of 2.28 Å.

Table 3
Adsorption properties of S on the close packed surfaces of various metals

	Site	E_{ads} (eV)	$d_{S-metal}$ (Å)
Ag(1 1 1)			
	Top	−2.81	2.29
	Bridge	–	–
	fcc	−3.94	2.45
	hcp	−3.88	2.46
Au(1 1 1)			
	Top	−2.49	2.25
	Bridge	−3.58	2.36
	fcc	−3.99	2.39(2.4)[a]
	hcp	−3.80	2.41
Cu(1 1 1)			
	Top	−3.58	2.08
	Bridge	−4.61	2.18
	fcc	−4.75	2.22
	hcp	−4.71	2.22
Ir(1 1 1)			
	Top	−3.52	2.16
	Bridge	−4.92	2.26
	fcc	−5.57	2.31(2.28)[b]
	hcp	−5.48	2.30
Ni(1 1 1)			
	Top	−3.74	2.01
	Bridge	−5.05	2.09
	fcc	−5.31	2.14(2.13–2.23)[c]
	hcp	−5.22	2.14
Pd(1 1 1)			
	Top	−3.17	2.14
	Bridge	−4.79	2.19
	fcc	−5.17	2.24(2.23–2.28)[d]
	hcp	−5.11	2.24
Pt(1 1 1)			
	Top	−3.19	2.16
	Bridge	−4.71	2.24
	fcc	−5.38	2.28(2.24–2.28)[e]
	hcp	−5.13	2.28

Listed are the: adsorption energy per S atom (E_{ads}) and the S–metal bondlength ($d_{S-metal}$). Where comparison is available, experimental values are given in parenthesis.
[a] Ref. [52].
[b] Ref. [31].
[c] Ref. [35,78,79].
[d] Ref. [36,37,81].
[e] Ref. [41,42].

We are not aware of any experimental studies for which to compare our calculated site preference and geometrical parameters for S on Ag(1 1 1) and Cu(1 1 1).

DFT investigations of S adsorption on Ag(1 1 1), Au(1 1 1), Cu(1 1 1), Pt(1 1 1) and Pd(1 1 1) at θ_S = 0.25 ML were previously undertaken [75,82–84]. DFT studies of S adsorption on Ni(1 1 1) and Pd(1 1 1) at θ_S = 0.11 ML were also reported [56,57]. These calculations also identified the fcc hollow site as the most stable for S adsorption. The reported fcc site adsorption energy on Ni(1 1 1) and Pd(1 1 1) at θ_S = 0.11 ML are −5.17 and −5.02 eV, respectively [56,57]. The corresponding S–Ni and S–Pd bondlengths are 2.15 and 2.27 Å, respectively. Our calculated values of 2.14 and 2.24 Å are close to their prediction. For the adsorption energies, our computed values of −5.31 and −5.17 eV on Ni(1 1 1) and Pd(1 1 1), respectively, are somewhat larger which could be due to some differences between the calculational details underlying these two studies.

The corresponding adsorption energies for H and the distance of the adsorbed H to the neighboring metal atoms are summarized in Table 4. A general preference for hollow site adsorption was observed. The calculated H-metal distance in threefold sites varies from 1.71 to 1.93 Å. On Ag(1 1 1), Au(1 1 1), Cu(1 1 1), Ni(1 1 1) and Pd(1 1 1), the fcc site is favored but we note that the other threefold hcp site is competing with an energy difference of just $\leqslant$0.05 eV. In a previous DFT studies, the interaction of H with the metal surfaces

examined here at θ_H = 0.25 ML were reported [85]. The difference in H adsorption energy between the most stable fcc site and the next most stable hcp site was essentially found to be in the same energy range [85].

On Pt(1 1 1), our calculations show that H has a smooth potential energy surface. It binds on the top, bridge, fcc and hcp sites with adsorption energy of −2.78, −2.75, −2.80 and −2.74 eV, respectively, showing a slight preference for adsorption on the fcc site. The nearly flat energy surface exhibited by H on this surface was also found in previous DFT investigations [86–88] and experiments using HREELS and quasi-elastic helium atom scattering techniques (QHAS) [89,90]. For Ir(1 1 1), top site adsorption was found to be the most energetically favorable. It is favored by about 0.06 eV over the next most stable site (fcc). The determination of favorable atop configuration was also obtained in previous DFT works at a coverage of 0.25 ML on Ir(1 1 1) [85,91].

The predicted general preference of H for the hollow sites is consistent with available experimental studies. For example, on Pd(1 1 1), it was suggested that H occupies the fcc site [92]. The LEED measured H-Pd distance of 1.78–1.80 Å [92] compares well with our calculated value of 1.82 Å. On Ni(1 1 1), H was reported to occupy both hollow sites without detectable difference in the H–Ni bondlength between the two sites [93]. The LEED determined bondlength was found to be 1.84 ± 0.06 Å which is slightly larger than our predicted value of 1.71 Å for both hollow sites. On the basis of HREELS measurements, top site adsorption was determined for the unusual case of Ir(1 1 1) in agreement with our work and other DFT studies mentioned above. The general preference for threefold hollow sites observed for both S and H also suggests that the gas phase bonding trends are not followed by these atomic adsorbates on the surfaces studied here. S binds to at most two atoms in the gas phase while H typically forms one bond. Yet, both atoms generally prefer to bind on the threefold hollow sites.

Table 4
Adsorption properties of H on the close packed surfaces of various metals

	Site	E_{ads} (eV)	$d_{H-metal}$ (Å)
Ag(1 1 1)			
	Top	−1.67	1.67
	Bridge	−2.09	1.83
	fcc	−2.22	1.92
	hcp	−2.21	1.93
Au(1 1 1)			
	Top	−2.05	1.61
	Bridge	−2.22	1.79
	fcc	−2.29	1.90
	hcp	−2.25	1.90
Cu(1 1 1)			
	Top	−1.94	1.52
	Bridge	−2.44	1.66
	fcc	−2.58	1.74
	hcp	−2.57	1.75
Ir(1 1 1)			
	Top	−2.72	1.61
	Bridge	−2.62	1.81
	fcc	−2.66	1.92
	hcp	−2.61	1.90
Ni(1 1 1)			
	Top	−2.22	1.48
	Bridge	−2.67	1.63
	fcc	−2.81	1.71(1.84)[a]
	hcp	−2.80	1.71
Pd(1 1 1)			
	Top	−2.34	1.55
	Bridge	−2.76	1.72
	fcc	−2.91	1.82(1.78–1.80)[b]
	hcp	−2.86	1.81
Pt(1 1 1)			
	Top	−2.78	1.56
	Bridge	−2.75	1.77
	fcc	−2.80	1.87
	hcp	−2.74	1.87

Listed are the: adsorption energy per H atom (E_{ads}) and H–metal bondlength ($d_{H-metal}$) for H binding on the various close packed metal surfaces. Where comparison is available, experimental values are given in parenthesis.
[a] Ref. [93].
[b] Ref. [92].

3.2. H_2S dissociation on the metal surfaces

After the preferred adsorption sites for H_2S, SH, S and H were determined, we then mapped out the minimum energy pathway (MEP) for H_2S dissociation on the surfaces using the NEB method. As mentioned above, the following processes were considered: $H_2S_{(ad)} \rightarrow SH_{(ad)} + H_{(ad)}$ and $SH_{(ad)} \rightarrow S_{(ad)} + H_{(ad)}$. The NEB method requires that the initial reactants and final reaction products be determined beforehand. For the first dissociation step ($H_2S_{(ad)} \rightarrow SH_{(ad)} + H_{(ad)}$), we analyzed a path starting with the H_2S in its ground state position on the top site of the surfaces. For the final state, we chose a configuration which consists of a stable coadsorbed state of SH and H within the (3×3) surface cell. The dissociated fragments SH and H share the smallest number of surface metal atoms possible (principle of least atom sharing). On Ag(1 1 1), Au(1 1 1), Cu(1 1 1), Ni(1 1 1), and Pd(1 1 1), the coadsorbed state consists of SH on the bridge site and the H atom on the fcc site. On Ir(1 1 1) and Pt(1 1 1), the corresponding H atom is on the top site because it prefers this site on Ir(1 1 1) while the H top site adsorption on Pt(1 1 1) is nearly degenerate with the fcc site. For the second dissociation step ($SH_{(ad)} \rightarrow S_{(ad)} + H_{(ad)}$), the starting point was taken to be the most stable state of the adsorbed SH species. A stable coadsorbed state of the dissociated fragment was considered for the final state with S and H sharing the smallest number of substrate atoms possible. On Ag(1 1 1), Au(1 1 1), Cu(1 1 1), Ni(1 1 1), and Pd(1 1 1), S is on the fcc site while H is on a neighboring hcp site. The corresponding H on Ir(1 1 1) and Pt(1 1 1) is again located on the top site.

The initial, transition and final states for the calculated MEP for the dissociation processes on the different surfaces are depicted in Figs. 2–4. The reaction barriers, reaction energies along with selected geometric parameters at transition state are tabulated in Table 5. On the different studied metals, the $H_2S_{(ad)} \rightarrow SH_{(ad)} + H_{(ad)}$ pathway can be approximately divided into three steps: (i) A S–H bond breaks by bending the bond towards the surface, (ii) the dissociating H continues to move toward a nearby top or bridge site. The transition state is reached when the distance between the dissociating H and the SH fragment is $d_{S-H} \geqslant 1.42$ Å, (iii) after the transition state, the SH fragment tilts towards the surface and then ends up in a bridge configuration while dissociating H eventually ends up on its preferred adsorption site.

Except for Au(1 1 1), we found that the first dissociation step is energetically favorable over the different surfaces and the predicted energy change varies from −0.15 to −1.25 eV. On Au(1 1 1), this reaction step is slightly endothermic (ΔE_{rxn} = 0.02 eV). The computed energy barriers for the H abstraction on the transition metals are 0.07–0.22 eV. The barrier is found to be moderately higher on the noble metals (E_a = 0.43–0.86 eV). The transition state on the transition metals is structurally more reactant-like than product-like. The distance of the dissociating H from the S is elongated by 0.05–0.25 Å compared to the molecularly adsorbed H_2S. For the S–metal bond, the corresponding bondlength is reduced by 0.01–0.07 Å. On the other hand, the corresponding transition states on the noble metals are much farther from their positions in the reactant structure. The dissociating H is 1.83–2.47 Å away from the S at the transition state. The SH bondlength in the molecularly adsorbed H_2S is 1.36 Å which suggests that the dissociating H is practically abstracted from the SH fragment. The S–metal

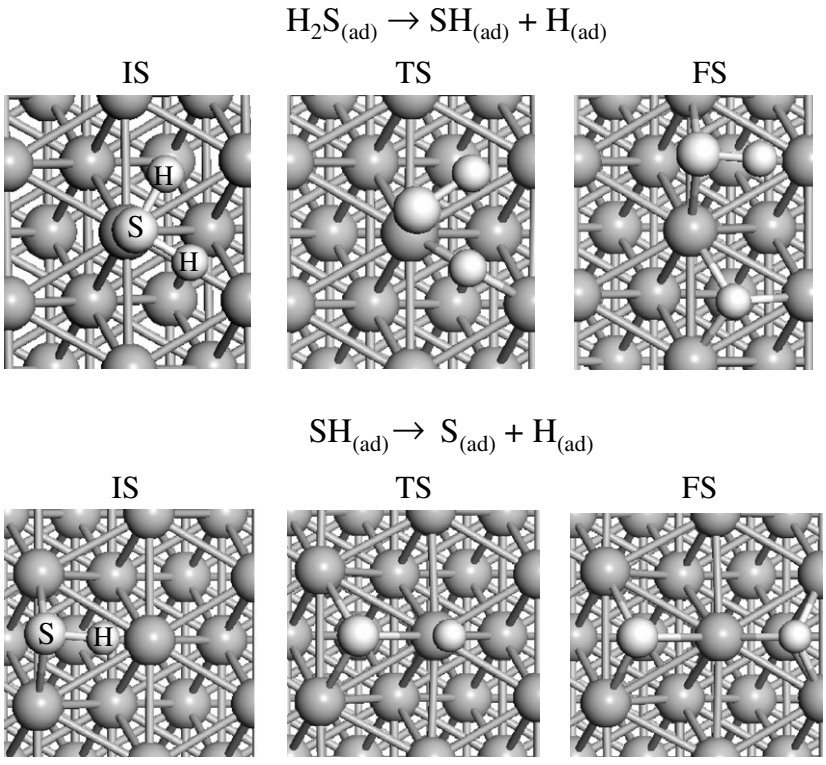

Fig. 2. Basic structure of the initial (IS), transition (TS) and final states (FS) for $H_2S_{(ad)} \rightarrow SH_{(ad)} + H_{(ad)}$ and $SH_{(ad)} \rightarrow S_{(ad)} + H_{(ad)}$ reactions on Ag(1 1 1), Au(1 1 1) and Cu(1 1 1).

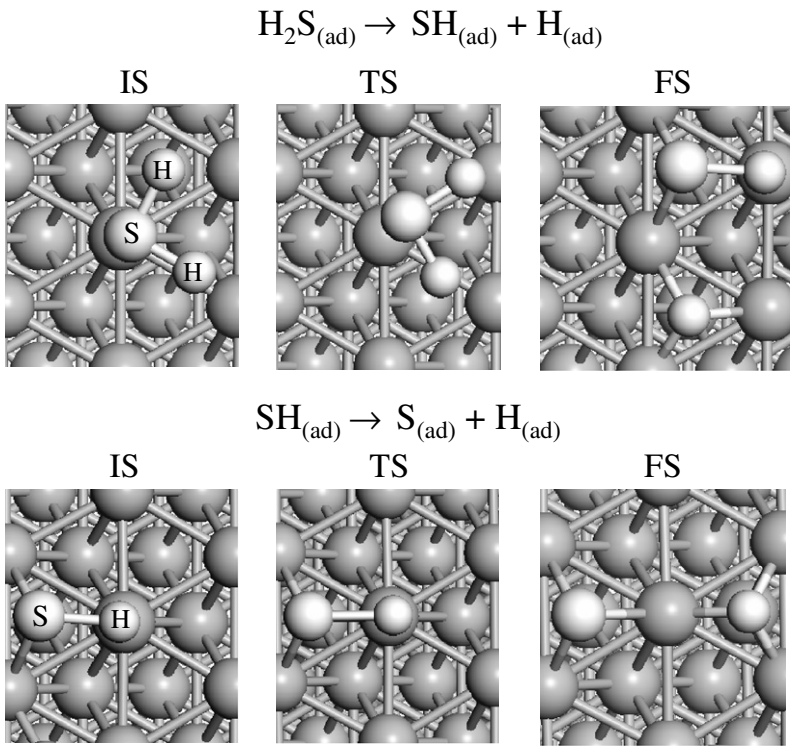

Fig. 3. Same as in Fig. 2 for $H_2S_{(ad)} \rightarrow SH_{(ad)} + H_{(ad)}$ and $SH_{(ad)} \rightarrow S_{(ad)} + H_{(ad)}$ reactions on Ni(1 1 1) and Pd(1 1 1).

bondlengths are 2.35–2.56 Å and they are reduced by 0.05–0.26 Å with respect to the adsorbed molecule.

The second dissociation pathway over the different metals studied essentially follows the general features of the first one. (i) The SH species moves towards the surface and points the H atom to a nearby metal atom. (ii) The H atom then moves away from the S fragment towards a nearby metal atom. The transition state is reached when the distance of the dissociating H atom from S is *d*

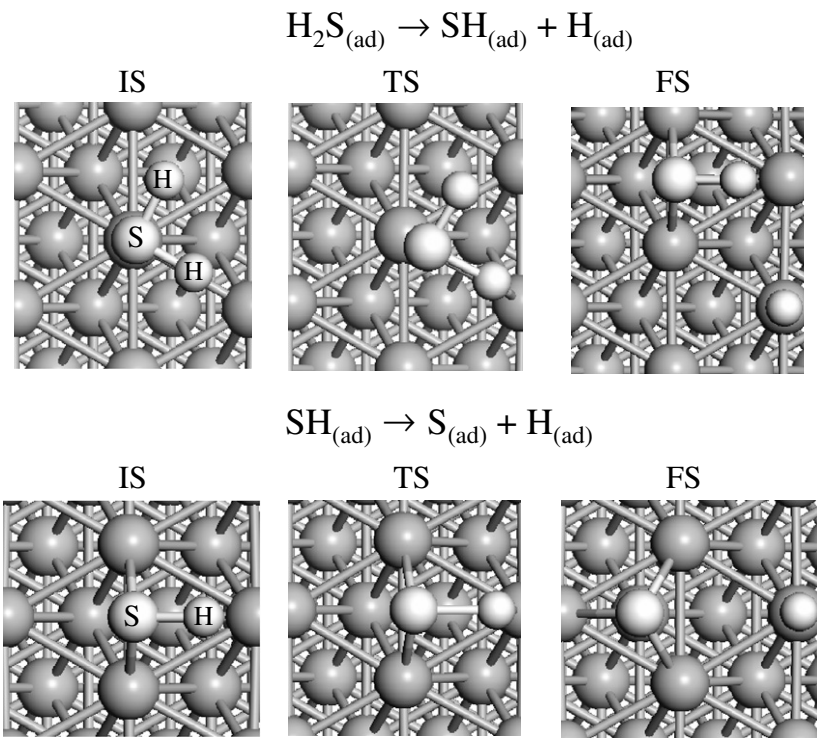

Fig. 4. Same as in Fig. 2 for $H_2S_{(ad)} \rightarrow SH_{(ad)} + H_{(ad)}$ and $SH_{(ad)} \rightarrow S_{(ad)} + H_{(ad)}$ reactions on Ir(1 1 1) and Pt(1 1 1).

Table 5
Reaction barrier (E_a), reaction energy (ΔE_{rxn}) and geometric parameters at the transition state for $H_2S_{(ad)} \rightarrow SH_{(ad)} + H_{(ad)}$ and $SH_{(ad)} \rightarrow S_{(ad)} + H_{(ad)}$ reactions on the various metal surfaces

	E_a (eV)	ΔE_{rxn} (eV)	d_{S-H} (Å)	$d_{S-metal}$ (Å)
Ag(1 1 1)				
$H_2S_{(ad)} \rightarrow SH_{(ad)} + H_{(ad)}$	0.86	−0.15	2.00(1.36)	2.56(2.82)
$SH_{(ad)} \rightarrow S_{(ad)} + H_{(ad)}$	1.06	0.12	2.16(1.37)	2.47(2.56)
Au(1 1 1)				
$H_2S_{(ad)} \rightarrow SH_{(ad)} + H_{(ad)}$	0.72	0.02	2.47(1.36)	2.41(2.62)
$SH_{(ad)} \rightarrow S_{(ad)} + H_{(ad)}$	0.68	0.02	2.24(1.37)	2.38(2.47)
Cu(1 1 1)				
$H_2S_{(ad)} \rightarrow SH_{(ad)} + H_{(ad)}$	0.43	−0.80	1.83(1.36)	2.35(2.40)
$SH_{(ad)} \rightarrow S_{(ad)} + H_{(ad)}$	0.40	−0.60	1.91(1.37)	2.24(2.47)
Ir(1 1 1)				
$H_2S_{(ad)} \rightarrow SH_{(ad)} + H_{(ad)}$	0.16	−1.02	1.62(1.37)	2.35(2.34)
$SH_{(ad)} \rightarrow S_{(ad)} + H_{(ad)}$	0.05	−1.07	1.69(1.40)	2.29(2.34)
Ni(1 1 1)				
$H_2S_{(ad)} \rightarrow SH_{(ad)} + H_{(ad)}$	0.21	−1.25	1.42(1.37)	2.27(2.21)
$SH_{(ad)} \rightarrow S_{(ad)} + H_{(ad)}$	0.01	−0.90	1.68(1.52)	2.16(2.17)
Pd(1 1 1)				
$H_2S_{(ad)} \rightarrow SH_{(ad)} + H_{(ad)}$	0.22	−0.88	1.57(1.37)	2.35(2.31)
$SH_{(ad)} \rightarrow S_{(ad)} + H_{(ad)}$	0.01	−0.82	1.54(1.44)	2.30(2.29)
Pt(1 1 1)				
$H_2S_{(ad)} \rightarrow SH_{(ad)} + H_{(ad)}$	0.07	−0.85	1.44(1.37)	2.31(2.30)
$SH_{(ad)} \rightarrow S_{(ad)} + H_{(ad)}$	0.03	−0.79	1.85(1.40)	2.26(2.31)

d_{S-H} is the sulfur-dissociating hydrogen distance while $d_{S-metal}$ is the sulfur–metal distance (values in parentheses refer to the initial state). A negative ΔE_{rxn} corresponds to an exothermic reaction.

$_{S-H} \geqslant 1.54$ Å. (iii) After the transition state, SH continues to come apart. The S fragment tilts towards the surface and ends in a fcc configuration while the dissociating H moves towards its preferred configuration. On the transition metals, the second dissociation step is a nearly spontaneous process with predicted energy barriers of $E_a \leqslant 0.05$ eV and energy change of $\Delta E_{rxn} = -0.79$ to -1.07 eV. The transition states are structurally more reactant-like. On Ir(1 1 1), Ni(1 1 1) and Pd(1 1 1) the S–H distance are stretched by 0.14–0.29 Å compared to initial adsorbed SH state. The S atom remains close to the bridge site with S–metal bondlengths reduced by only 0.01–0.05 Å compared to the initial state. On Pt(1 1 1), S also remains close to the bridge site though the S–H stretched is slightly more pronounced (0.45 Å). On the noble metals, the barriers are larger (0.40–1.06 eV). The corresponding reaction energies are 0.12, 0.02 and −0.60 eV on Ag(1 1 1), Au(1 1 1) and Cu(1 1 1), respectively. At the transition state, the S–H distance (1.91–2.24 Å) is very different to that of the initial state (1.37 Å). This indicates that on the different noble metals studied here, H is essentially abstracted from the S fragment. Additionally, the S atom is close to the fcc site as it formed a bond with the nearby metal atom where the H atom moved to.

A detailed energy profile for the dissociation of adsorbed H_2S is presented in Fig. 5. The overall thermochemistry of each reaction step is calculated by considering a case of infinite separation between $SH_{(ad)}$ and $H_{(ad)}$ or $S_{(ad)}$ and $H_{(ad)}$. In this situation, there is no repulsion between the dissociated products. We found that the overall decomposition process on the various metals is exothermic. In general, the first dissociation step on the different metals has a higher energy barrier compared to the second one. The energy barrier for both elementary steps on the transition metals is smallest while the barrier on the noble Ag(1 1 1) and Au(1 1 1) surfaces is significantly larger. That of H_2S on Cu(1 1 1) lies in between. Thus, the close packed transition metal surfaces considered here are more efficient in dissociating H_2S. The lower barriers on the transition metals may be at least partially attributed to the fact that H_2S and SH are more strongly bound on these particular surfaces. For H_2S, the adsorption energies are −0.56 to −0.91 eV compared to −0.17 to −0.27 eV for noble metals (see Table 1). In the case of SH, the values are −3.18 to −3.37 eV compared to −2.23 to −2.76 eV (see Table 2). This means that H_2S and SH adsorbed on the transition metals have a more weakened S–H bond already before dissociation. Thus, it requires less energy to reach the transition state, leading to a lower barrier.

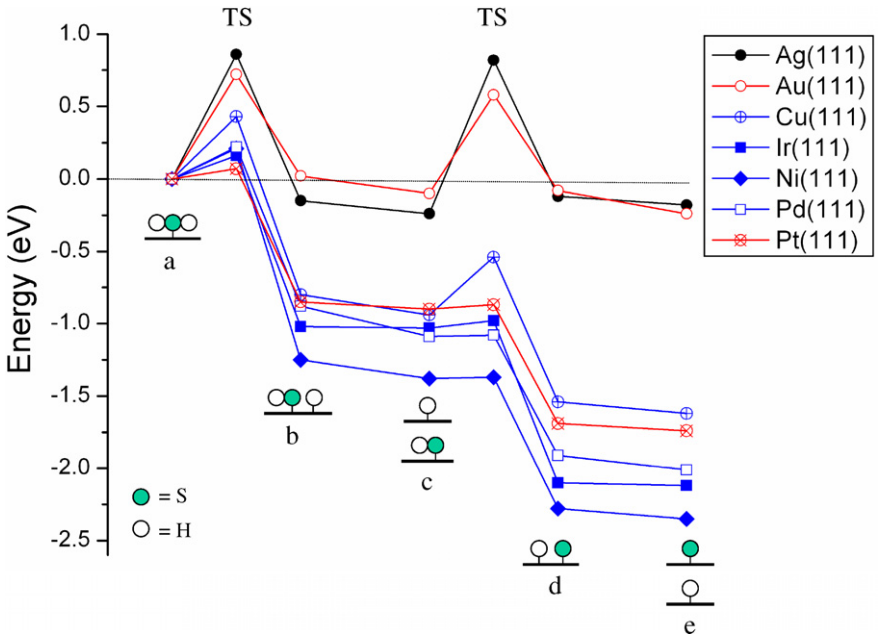

Fig. 5. Relative energy diagram for H_2S decomposition on the various metal surfaces. The states labeled (a), (b) and (d) correspond to adsorbed H_2S, dissociated H_2S and dissociated SH, respectively. The state labeled (c) and (e) correspond to SH + H and S + H chemisorbed in separate surface unit cells.

The decomposition of H_2S results in pronounced changes in the metal substrates electronic structure. This is illustrated in Figs. 6 and 7 by the partial electronic density of states (PDOS) of the initial and final states of $H_2S_{(ad)} \rightarrow SH_{(ad)} + H_{(ad)}$ and $SH_{(ad)} \rightarrow S_{(ad)} + H_{(ad)}$ reactions on transition metal Pd(1 1 1) surface. We only show results for this representative case for the sake of keeping the paper within a limited length. For adsorbed H_2S, broad peaks centered around −7.4 and −6.2 eV and a diffuse feature in the energy range −5.0 to −4.0 eV (electronic energies are given with respect to the Fermi level) are found in the S p PDOS (Fig. 6). The peak around −7.4 eV has a discernable overlap with H s which can be considered as a marker of S–H bonds in the adsorbed H_2S. The PDOS of the metal substrate, on the other hand, consists of extended and broad d band that embraces the Fermi level. The d states close to the bottom of the d band plus the d split-off states overlap in energy with features that have mainly S p character. This hybridization is consistent with the fact the H_2S interacts with the surface primarily through the S atom. Upon dissociation of the molecule to $SH_{(ad)} + H_{(ad)}$, a different adsorption character is clearly observable in the corresponding PDOS. The dissociation of one of the H atoms has caused the feature inherent to the S–H bond in H_2S to disappear. A portion of the PDOS of Pd(1 1 1) is energetically stabilized (i.e. shifted to lower energies). At the same time, the main S p peaks are shifted to higher energies which results into an enhancement in the hybridization between Pd d and S p. Moreover, the S p states are now found to hybridize with the substrate d states over the range of the whole d band. This is consistent with the more pronounced S–Pd interaction after the abstraction of H from the adsorbed H_2S. There is also a discernable overlap between the Pd split-off d states and the H s states as a result of enhanced interaction of H with the metal substrate.

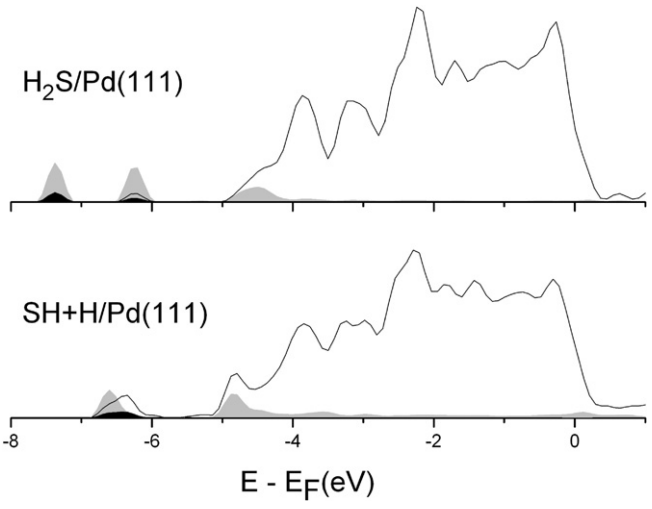

Fig. 6. PDOS ($E_F = 0$) for H_2S and SH + H on Pd(1 1 1). Gray shaded areas correspond to S p PDOS. Black shaded areas correspond to H s PDOS. Solid line corresponds to Pd d PDOS.

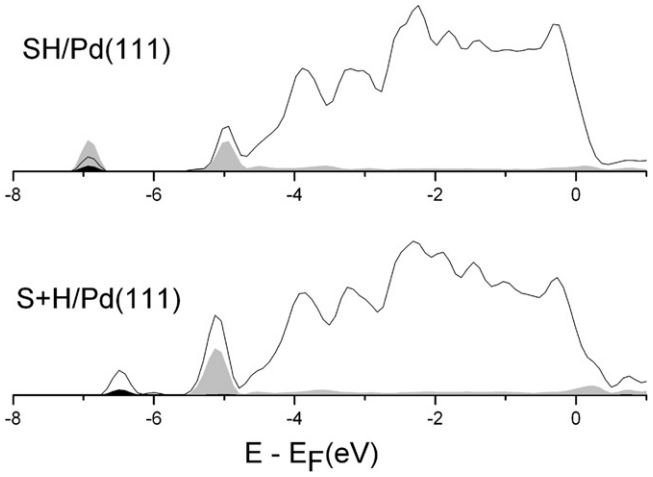

Fig. 7. PDOS ($E_F = 0$) for SH and S + H on Pd(1 1 1). Gray shaded areas correspond to S p PDOS. Black shaded areas correspond to H s PDOS. Solid line corresponds to Pd d PDOS.

For the adsorbed SH (Fig. 7), they show some resemblance to that of the $SH_{(ad)} + H_{(ad)}$ except that the overlapping Pd d, S p and

H s states are shifted to lower energies. The hybridization between Pd d and S p are also more pronounced in comparison. This is consistent with the stronger interaction between S (in adsorbed SH) and Pd as a result of the absence of a neighboring adsorbed H. For the dissociated state, $S_{(ad)} + H_{(ad)}$ where the S fragment forms a strong bond with the surface, the interaction of the adsorbates with the surface gives rise to a relatively well developed overlapping feature around −5.1 eV. This consists of hybridization of Pd d and S p states. It should be noted that this feature is inherent for S adsorption on Pd(1 1 1) and was suggested as a marker for the strong covalent bond between the S and the metal substrate [94,95]. While there is a discernible overlap between the occupied states of H and the substrate, virtually none is observed between S and H as a result of the cleavage of the S–H bond.

Experimental studies of H_2S adsorbed on the clean Ag(1 1 1), Au(1 1 1), Cu(1 1 1) and Pt(1 1 1) in UHV were previously reported. In the TPD studies on Ag(1 1 1) and Au(1 1 1) surfaces, it was found that the molecule merely desorbs without reaction [7,8]. Decomposition on Ag(1 1 1) was only seen when the surface contains preadsorbed sulfur while on Au(1 1 1), the dissociation was facilitated by electron stimulated decomposition of the adsorbed H_2S. In the case of Cu(1 1 1), dissociation was not observed at low temperatures [10]. At $T = 200$ K, it was found that some of the molecule starts to desorb and the rest dissociates. After further heating to 300 K, the dissociation of the molecule becomes the most dominant process. The adsorption energy calculated here for the molecule on Ag(1 1 1) and Au(1 1 1) are −0.17 and −0.27 eV, respectively, while the data in Fig. 5 demonstrates that the corresponding reaction barrier for the dissociation process is 1.06 (Ag(1 1 1)) and 0.72 eV (Au(1 1 1)). Thus, H_2S desorption would preferentially occur in agreement with experiments. On Cu(1 1 1), the H_2S adsorption energy is comparable to that of Au(1 1 1) but the corresponding barrier is noticeably lower ($E_a = 0.43$ eV vs. $E_a = 1.06$) This could be the reason why the dissociation process on Cu(1 1 1) becomes more competitive with increasing temperature in comparison to Ag(1 1 1) and Au(1 1 1). This is in contrast with Pt(1 1 1) on which the dissociation of H_2S was found to be more facile. On the clean Pt(1 1 1) surface, dissociation occurs following H_2S adsorption at 110 K [11]. The ease of dissociation on Pt(1 1 1) in comparison to the noble metals could be explained by our calculations. The calculated adsorption energy for H_2S is −0.91 eV while the dissociation barrier is at least 0.07 eV. The overall dissociation process was also found to have high exothermicities. Hence, adsorbed H_2S that forms on Pt(1 1 1) will preferentially dissociate.

In a previous DFT work, the dissociation of H_2S on Ni(1 1 1) at $\theta_{H_2S} = 1/9$ ML was examined [57]. The reaction paths they examined are consistent with that considered here. The barriers (0.22 and 0.01 eV) and reaction energies (−1.25 and −0.89 eV) they predicted for the first and second dissociation step compare very well with our results. The dissociation of H_2S on Pd(1 1 1) at $\theta_{H_2S} = 1/16$ ML was the subject of DFT investigations [56]. The calculated barriers for the first and second dissociation step are 0.37 and 0.04 eV, respectively. The present work yields 0.22 and 0.01 eV, respectively. It should be noted that the pathway we found here for the first dissociation step has a lower barrier. In the present work, the final state for the first dissociation step corresponds to an adsorbed SH and an adsorbed H atom on a next nearest neighbor hollow site. In the earlier work, the dissociating H was moving towards a more remote hollow site (about two nearest neighbor atomic distance away) during the abstraction process. At the transition state of this less favorable pathway, the dissociating H was practically abstracted from the SH fragment. This is not the situation for the pathway that was examined here. The dissociation properties of H_2S on Pt(1 1 1) was also reported from a previous DFT investigations [75]. The studies were done at a higher coverage ($\theta_{H_2S} = 1/4$ ML). The initial and final states of the first and second dissociation steps are similar to our studies. Both H_2S and SH were found to have low abstraction barriers (<0.1 eV) and high exothermicities (∼−1 eV) on Pt(1 1 1) suggesting that the dissociation process is a facile process. Our results at lower coverage also indicate that this process is kinetically and thermodynamically favorable.

4. Conclusion

In summary, the results of first-principles density functional theory investigations addressing the adsorption and dissociation of H_2S on Ag(1 1 1), Au(1 1 1), Cu(1 1 1), Ir(1 1 1), Ni(1 1 1), Pd(1 1 1) and Pt(1 1 1) surfaces were reported. We determined site preferences, binding geometries and adsorption energies of H_2S and the various intermediates (SH, S and H). For H_2S, molecular adsorption is found to be energetically favorable. The molecule is quite weakly adsorbed, favoring the top site and with the molecular plane lying parallel to the substrate. In comparison, SH, S and H interact strongly with the surfaces. SH preferentially adsorbs on the bridge site with the axis of the molecule nearly parallel to the surface. For atomic S and H, adsorption on the threefold hollow sites is generally preferred. The binding of H_2S and its S-containing dissociated species is stronger on the transition metal surfaces (Ir(1 1 1), Ni(1 1 1), Pd(1 1 1) and Pt(1 1 1)) than on the noble metal surfaces (Ag(1 1 1), Au(1 1 1) and Cu(1 1 1)).

Minimum energy pathways and energy profiles for the (i) decomposition of H_2S into adsorbed SH and H, and (ii) the decomposition of SH into adsorbed S and H were determined. On the different metals, the predicted pathway for both dissociation process can be approximately divided into three steps. Initially, the adsorbate points the S–H bond towards the surface. Then, the dissociating H atom moves towards a nearby metal atom. At the transition state, the S–H bond starts to break. As the adsorbate comes apart, both the dissociating H and the S-containing fragment move towards their most preferred configuration. Overall, the decomposition process on the various metals is predicted to be exothermic. However, the barrier for both dissociation steps on Ag(1 1 1) and Au(1 1 1) is significantly higher. The barrier on Ir(1 1 1), Ni(1 1 1), Pd(1 1 1) and Pt(1 1 1) is much smaller while that on Cu(1 1 1) lies in between. Our studies suggest that the close packed transition metal surfaces examined here are more efficient in dissociating H_2S.

Acknowledgements

We are grateful to D. Sorescu for useful discussions. This technical effort is under NETL Contract DE-AM26-04NT41817, Subtask 41817.660.01.01.

References

[1] R.R. Chianelli, in: J.P. Bonnelle (Ed.), Surface Properties and Catalysis by Non-metals, Reidel, Dordrecht, 1983, p. 361.
[2] M. Ando, T. Suto, T. Suzuki, C. Tsuchida, C. Nakayama, N. Miura, N. Yamazoe, Chem. Lett. 335 (1994).
[3] K. Soo Yoo, I.W. Sorenson, W.S. Glaunsinger, J. Vac. Sci. Technol. A 12 (1994) 192.
[4] F. Roa, J.D. Way, R.L. McCormick, S.N. Paglieri, Chem. Eng. J. 93 (2003) 11.
[5] S. Adhikari, S. Fernando, Ind. Eng. Chem. Res. 45 (2006) 875.
[6] J.A. Rodriguez, J. Hrbek, Acc. Chem. Res. 32 (1999) 719.
[7] Y. Yu, S.J. Dixon-Warren, N. Astle, Chem. Phys. Lett. 312 (1999) 455.
[8] A.J. Leavitt, T.P. Beebe Jr., Surf. Sci. 314 (1994) 23.
[9] J. Lahtinen, P. Kantola, S. Jaatinen, K. Habermehl-Cwirzen, P. Salo, J. Vuorinen, M. Lindroos, K. Pussi, A.P. Seitsonen, Surf. Sci. 599 (2005) 113.
[10] C.T. Campbell, B.E. Koel, Surf. Sci. 183 (1987) 100.
[11] R.J. Koestner, M. Salmeron, E.B. Kollin, J.L. Gland, Chem. Phys. Lett. 125 (1986) 134.
[12] G. Rovida, F. Pratesi, Surf. Sci. 104 (1981) 609.
[13] M.P. Sotto, J.C. Boulliard, Surf. Sci. 162 (1985) 285.
[14] D.M. Jaffey, R.J. Madix, Surf. Sci. 314 (1991) 23.
[15] B. Fruhberger, M. Grunze, D.J. Dwyer, J. Phys. Chem. 98 (1998) 609.

[16] V. Bondzie, S.J. Dixon-Warren, Y. Yu, J. Chem. Phys. 111 (1999) 10670.
[17] K.T. Leung, X.S. Zhang, D.A. Shirley, J. Phys. Chem. 93 (1989) 6164.
[18] J.L. Gland, E.B. Kollin, F. Zaera, Langmuir 4 (1988) 118.
[19] A.G. Baca, M.A. Schulz, D.A. Shirley, J. Chem. Phys. 81 (1984) 6304.
[20] Y. Zhou, J.M. White, Surf. Sci. 183 (1987) 363.
[21] R. McGrath, A.A. MacDowell, T. Hashizume, F. Sette, P.H. Citrin, Phys. Rev. B 40 (1989) 9457.
[22] D.R. Huntley, Surf. Sci. 240 (1990) 13.
[23] W. Berndt, R. Hora, M. Scheffler, Surf. Sci. 117 (1982) 188.
[24] R.I. Hedge, J.M. White, J. Phys. Chem. 90 (1986) 296.
[25] G.B. Fischer, Surf. Sci. 87 (1979) 215.
[26] A.K. Battacharaya, L.J. Clarke, L. Morales de la Garza, J. Chem. Soc. Faraday Trans. 1 (77) (1981) 2223.
[27] S.R. Kelemen, T.E. Fischer, Surf. Sci. 87 (1979) 53.
[28] D. Jürgens, G. Held, H. Pfnür, Surf. Sci. 303 (1994) 77.
[29] R. Dennert, M. Solokpwski, H. Pfnür, Surf. Sci. 271 (1992) 1.
[30] D. Heuer, T. Müller, H. Pfnür, U. Kohler, Surf. Sci. Lett. 297 (1993) L61.
[31] C.M. Chan, W.H. Weinberg, J. Chem. Phys. 71 (1979) 3988.
[32] M. Perdereau, J. Oudar, Surf. Sci. 20 (1970) 80.
[33] Y.K. Wu, K.A.R. Mitchell, Can. J. Chem. Eng. 67 (1989) 1975.
[34] J. Luedecke, A.R.H.F. Ettema, S.M. Driver, G. Scragg, M. Kerkar, D.P. Woodruff, B.C.C. Cowie, R.G. Jones, S. Bastow, Surf. Sci. 366 (1996) 260.
[35] D.R. Warburton, P.L. Wincott, G. Thornton, F.M. Quinn, D. Norman, Surf. Sci. 211/212 (1989) 71.
[36] F. Maca, M. Scheffler, W. Berndt, Surf. Sci. 160 (1985) 467.
[37] M.E. Grillo, C. Stampfl, W. Berndt, Surf. Sci. 317 (1994) 84.
[38] W. Liu, K.A.R. Mitchell, W. Berndt, Surf. Sci. 393 (1997) L119.
[39] S. Speller, T. Rauch, A. Postnikov, W. Heiland, Phys. Rev. B 61 (2000) 7297.
[40] C.H. Patterson, R.M. Lambert, Surf. Sci. 187 (1987) 339.
[41] H.A. Yoon, N. Materer, M. Salmeron, M.A.V. Hove, G.A. Somorjai, Surf. Sci. 376 (1997) 254.
[42] K. Hayek, H. Glassl, A. Gutmann, H. Leonhard, M. Prutton, S.P. Tear, M.R. Welton-Cook, Surf. Sci. 152/153 (1985) 419.
[43] K. Hayek, H. Glassl, A. Gutmann, H. Leonhard, M. Prutton, S.P. Tear, M.R. Welton-Cook, Surf. Sci. 175 (1986) 535.
[44] J.A. Rodriguez, J. Hrbek, M. Kuhn, T. Jirsak, S. Chatuverdi, J. Chem. Phys. 113 (2000) 11284.
[45] K.C. Wong, W. Liu, M. Saidy, K.A.R. Mitchell, Surf. Sci. 345 (1996) 101.
[46] H.A. Yoon, M. Salmeron, G.A. Somorjai, Surf. Sci. 395 (1998) 268.
[47] A. Santoni, B.C.C. Cowie, G. Scarel, V.R. Dhanak, Surf. Sci. 388 (1997) 254.
[48] G.D. Aloisi, M. Cavallini, M. Innocenti, L. Foresti, G. Pezzatini, R. Guidelli, J. Phys. Chem. B 101 (1997) 4774.
[49] R. Heinz, J.P. Rabe, Langmuir 11 (1995) 506.
[50] B.K. Min, A.R. Alemozafar, M.M. Biener, J. Biener, C.M. Friend, Topics in Catal. 36 (2005) 77.
[51] X. Gao, Y. Zhang, M.J. Weaver, J. Phys. Chem. B 96 (1992) 4156.
[52] C. Vencat, M.E. Vela, G.A. Benitez, J.A.M. Gago, X. Torrelles, R.C. Salvarezza, J. Phys. Condens. Matter 18 (2006) R867.
[53] M.D. Craper, C.E. Riley, P.J. Sweeney, C.F. McConville, D.P. Woodruff, R.G. Jones, Surf. Sci. 182 (1987) 213.
[54] E. Wahlstrom, I. Ekvall, H. Olin, S.A. Lindgren, L. Wallden, Phys. Rev. B 60 (1999) 10699.
[55] M. Saidy, K.A.R. Mitchell, Surf. Sci. 441 (1999) 425.
[56] D.R. Alfonso, A.V. Cugini, D.C. Sorescu, Catal. Today 99 (2005) 315.
[57] E.J. Albenze, A. Shamsi, Surf. Sci. 600 (2006) 3202.
[58] D.E. Jiang, E.A. Carter, J. Phys. Chem. B 108 (2004) 19140.
[59] D.E. Jiang, E.A. Carter, Surf. Sci. 583 (2005) 60.
[60] G. Kresse, J. Hafner, Phys. Rev. B 49 (1994) 14251.
[61] G. Kresse, J. Fürthmuller, Phys. Rev. B 54 (1996) 11169.
[62] J.P. Perdew, K. Burke, M. Enzerhof, Phys. Rev. Lett. 77 (1996) 3865.
[63] G. Kresse, D. Joubert, Phys. Rev. B 59 (1999) 1758.
[64] C. Kittel, Introduction to Solid State Physics, sixth ed., Wiley, NY, 1986.
[65] J. Neugebauer, M. Scheffler, Phys. Rev. B 46 (1992) 16067.
[66] H.J. Monkhorst, J.D. Pack, Phys. Rev. B 13 (1976) 5188.
[67] M. Methfessel, A.T. Paxton, Phys. Rev. B 40 (1989) 3616.
[68] J.P. Perdew, J.A. Chevary, S.H. Vosko, K.A. Jackson, M. Pederson, D.J. Singh, C. Fiolhais, Phys. Rev. B 46 (1992) 6671.
[69] G. Kresse, J. Hafner, J. Phys. Condens. Matter 6 (1994) 8245.
[70] G. Mills, H. Jönsson, G. Schenter, Surf. Sci. 324 (1995) 305.
[71] G. Henkelman, B.P. Uberuaga, H. Jönsson, J. Chem. Phys. 113 (2000) 9901.
[72] A. Michealides, P. Hu, J. Am. Chem. Soc. 122 (2000) 9866.
[73] Y.M. Choi, C. Compson, M.C. Lin, Chem. Phys. Lett. 421 (2006) 179.
[74] N.M. Galea, E.S. Kadantsev, T. Ziegler, J. Phys. Chem. C 111 (2007) 14457.
[75] A. Michaelides, P. Hu, J. Chem. Phys. 115 (2001) 8570.
[76] D. Alfe, M.J. Gillan, J. Phys. Condens. Matter 18 (2006) L451.
[77] M. Pozzo, G. Carlini, R. Rosei, D. Alfe, J. Chem. Phys. 126 (2007) 164706.
[78] Y. Kitajima, S. Yagi, T. Yokoyama, A. Imanishi, S. Takemaka, T. Ohta, Surf. Sci. 320 (1994) L89.
[79] Y. Ku, S.H. Overbury, Surf. Sci. 276 (1992) 262.
[80] J.E. Demuth, Chem. Phys. Lett. 45 (1977) 12.
[81] V.R. Dhanak, A.G. Shard, B.C.C. Cowie, A. Santoni, Surf. Sci. 410 (1998) 321.
[82] D.R. Alfonso, A.V. Cugini, D.S. Sholl, Surf. Sci. 546 (2003) 12.
[83] J. Gottschalck, B. Hammer, J. Chem. Phys. 116 (2002) 784.
[84] M. Mavrikakis, J. Rempel, J. Greeley, L.B. Hansen, J.K. Nørskov, J. Chem. Phys. 117 (2002) 6737.
[85] J. Greeley, M. Mavrikakis, J. Phys. Chem. B 109 (2005) 3460.
[86] J. Greeley, M. Mavrikakis, J. Am. Chem. Soc. 124 (2002) 7193.
[87] A. Michaelides, P. Hu, J. Am. Chem. Soc. 128 (2001) 4235.
[88] G.W. Watson, R.P.K. Wells, D.J. Willock, G.J. Hutchings, J. Phys. Chem. B 105 (2001) 4889.
[89] A.P. Graham, A. Menzel, J.P. Toennies, J. Chem. Phys. 111 (1999) 1676.
[90] L.J. Richter, W. Ho, Phys. Rev. B 36 (1987) 9797.
[91] W.P. Krekelberg, J. Greeley, M. Mavrikakis, J. Phys. Chem. B 108 (2004) 987.
[92] T.E. Felter, E.C. Sowa, M.A. van Hove, Phys. Rev. B 40 (1989) 891.
[93] K. Christmann, R.J. Behm, G. Ertl, M.A. van Hove, W.H. Weiberg, J. Chem. Phys. 70 (1979) 4168.
[94] P.A. Gravil, H. Toulhoat, Surf. Sci. 430 (1999) 176.
[95] D.R. Alfonso, Surf. Sci. 596 (2005) 229.
[96] J.M.W. Chase, NIST-JANAF Thermochemical Tables, vol. 1, Hemisphere, New York, 1989.